Rev.Adv.Mater.Sci. 13 (2006) 47-58

DYNAMIC CRACK INITIATION AND PROPAGATION IN NANOCOMPOSITE MATERIALS

Arun Shukla[1], Venkitanarayanan Parameswaran[2], Ying Du[1] and Victor Évora[3]

[1]Dynamic Photomechanics Laboratory, Dept of Mechanical Engineering and Applied Mechanics, University of Rhode Island, Kingston, RI. 02881, USA
[2]Dept of Mechanical Engineering, Indian Institute of Technology, Kanpur, India 208016
[3]Naval Undersea Warfare Center Division, Newport, RI. 02841, USA

Received: August 02, 2006

Abstract. A comprehensive series of experiments is conducted to study dynamic crack initiation and propagation in nanocomposite materials. The nanocomposites are fabricated using ultrasonics with an *in-situ* polymerization technique to produce materials with excellent particle dispersion, as verified by transmission electron microscopy and scanning electron microscopy. Dynamic fracture toughness testing is carried out on three-point bend nanocomposite specimens using a modified split-Hopkinson pressure bar, and the results are compared to those of the matrix materials. Dynamic photoelasticity coupled with high speed photography has also been used to obtain crack tip velocities and dynamic stress fields around the propagating cracks. A relationship between the dynamic stress intensity factor, K_D, and the crack tip velocity, $\dot{a}$, is established.

1. INTRODUCTION

Engineering applications of thermosetting polymers are on the rise. Polymers such as polyester and epoxy are extensively used for applications ranging from consumer products, packaging, electronic circuits boards, boat building and building construction. Apart from the above applications these two thermosetting resins are the most commonly used matrix material in fiber composites, which have become quite a match for metals in terms of strength and stiffness. The high strength to weight ratio of such composites makes them even more favorites in aerospace applications. However, these highly cross-linked resins are extremely brittle owing to their covalently bonded network structure, and are thus poor inhibitors of crack initiation and propagation. Lack of tolerance of these resins to fracture oriented failure is a grave concern given the fact that the fracture failure of fiber composites is more dominated by matrix fracture than reinforcement failure.

Conventionally, there have been numerous studies attempting to improve the fracture toughness of thermosetting resins by adding rigid (metal and metal oxide) or flexible (rubber) micro particles to the polymers [1-5]. Addition of either type of particle will improve the fracture resistance of the resin, however, rigid particles reduce the tensile strength and failure strain of the resin whereas flexible particles reduce the stiffness of the resin, which are both undesirable. Recent availability of particles in the nanometer size range has motivated material scientists to investigate the effect of adding such reinforcements on the fracture behavior of thermosetting resins. Singh *et al*. [6] have investigated the effect of particle size ranging from 100 nanometers to 20 micrometers on the fracture toughness of polyester resin. Their results indicate that by using very small amount of nanometer size particles, the fracture toughness can be improved as much as 50% without reduction in strength. Zhang [7] achieved further improvements in fracture toughness by coating the nano particles with silane, which improved the interfacial adhesion between the particles and the matrix.

Corresponding author: Arun Shukla, e-mail: shuklaa@egr.uri.edu

In a subsequent investigation, Evora and Shukla [8] achieved a 60% improvement in fracture toughness of polyester resin by adding very low amount of 35 nm TiO_2 particles. They also determined the dynamic initiation toughness of the material. In a very recent study, Zunjarrao *et al.* [9] achieved a 35% increase in the fracture toughness of epoxy by adding nanoclay. These studies indicate that, compared to micron sized particles, nanometer size particles are better alternatives to improve the fracture toughness of thermosetting resins as they do not affect the tensile strength as adversely as the micron sized particles do.

When a crack is loaded quasi-statically, due to the presence of the particles there will be crack pinning and crack bridging within the fracture process zone. This allows stable crack extension at local particle sites before unstable fracture. These mechanisms alleviate the stress intensity levels locally allowing the material to withstand higher load before failure thereby registering an increase in fracture toughness. Dynamic fracture, on the other hand, is a sequence of events starting with crack initiation, followed by crack propagation and subsequently crack arrest or crack branching. Crack initiation can be under slow loading or dynamic loading. In the former case, crack initiation is characterized by the quasi-static fracture toughness whereas in the later case the dynamic initiation toughness characterizes the fracture initiation. If determined from proper experiments, both these quantities are material parameters for a given loading rate.

The crack propagation phase is characterized by the $\dot{a}$-K_D relationship, which indicates how the crack speed ($\dot{a}$) and the dynamic stress intensity factor (DSIF), K_D, are related. The speed of crack propagation, the distance propagated and whether there will be crack arrest eventually or crack branching will be dictated by the relative dominance of the energy available for crack propagation over the energy consumed in crack extension. While the former depends on the test conditions such as geometry of the specimen, loading etc. the later is entirely a material dependent factor. Under proper testing conditions of testing the arrest toughness, which is the dynamic stress intensity factor prior to crack arrest, is a material property. For unreinforced polyester and epoxy, the dynamic initiation toughness, $\dot{a}$-K_D relationship and the arrest toughness are already characterized [10,11]. In the case of nanocomposites, the particles act as obstacles to the propagating crack front and for continued crack extension the crack will have to either circumvent the particle or deflect along the particle matrix interface and switch to another plane. These additional mechanisms can alter the fracture characteristics altogether. Understanding of the principles governing dynamic fracture is of great importance, as it lends insight as to how the catastrophic failure can be stopped, or at the very least, subdued.

The work presented in this paper examines the fracture behavior of two thermosetting resin, polyester and epoxy, with three different types of reinforcements 1) TiO_2 spherical particles of 36 nm diameter; 2) Al_2O_3 spherical particles of 14 nm diameter and 3). High aspect ratio (25-50) Al_2O_3 platelets of 200 nm thickness. A comprehensive series of experiments is carried out to determine the effect of 1% volume fraction of these reinforcements on the quasistatic fracture toughness, dynamic initiation toughness, arrest toughness, and the $\dot{a}$-K_D relationship. The preparation of these composites is explained in the next section followed by the characterization of the quasi-static and dynamic initiation toughness. The experimental scheme used to study the propagation and arrest behavior is then briefly presented. The results are then discussed and the conclusions are highlighted.

2. NANOCOMPOSITE FABRICATION

The thermosetting resins polyester and epoxy (LY556), used in the study, are available as liquid monomer and can be easily polymerized by adding a catalyst or hardener. This system therefore is amenable to preparing nanocomposites by the technique of in-situ polymerization where the reinforcements are first dispersed in the liquid monomer and the mixture is subsequently polymerized to form the composite. However, the nano particles as received are highly agglomerated and these agglomerates have to be broken down and the individual particles dispersed uniformly in the resin. Different approaches based on either a chemical route or mechanical route are available, and in the present study direct mixing of the particles in the resin by sonication is followed. The resin and reinforcement system used in this study are listed in Table 1.

The 35 nm size TiO_2 particles have 40 m^2 surface area per gram of particle whereas the 14 nm size Al_2O_3 particles have 100 m^2 surface area per gram of particle. The Al_2O_3 platelets have polygonal shape with a thickness of 200 nm and in plane size of 5 to 10 micrometer. These have a surface are of 2.5 m^2 per gram of platelet. The nanoparticles/platelets were added to 230 grams of resin at the re-

Table 1. Material system used to prepare nanocomposites.

Resin	Polyester (MR17090)*		Epoxy (LY556)**
Reinforcement	TiO_2 (35 nm-spherical)	Al_2O_3 (14 nm-spherical)	Al_2O_3 platelets (200 nm thick)

*Supplied by Ashland Chemical Company, USA
** Supplied by Vantico Performance Polymers, India

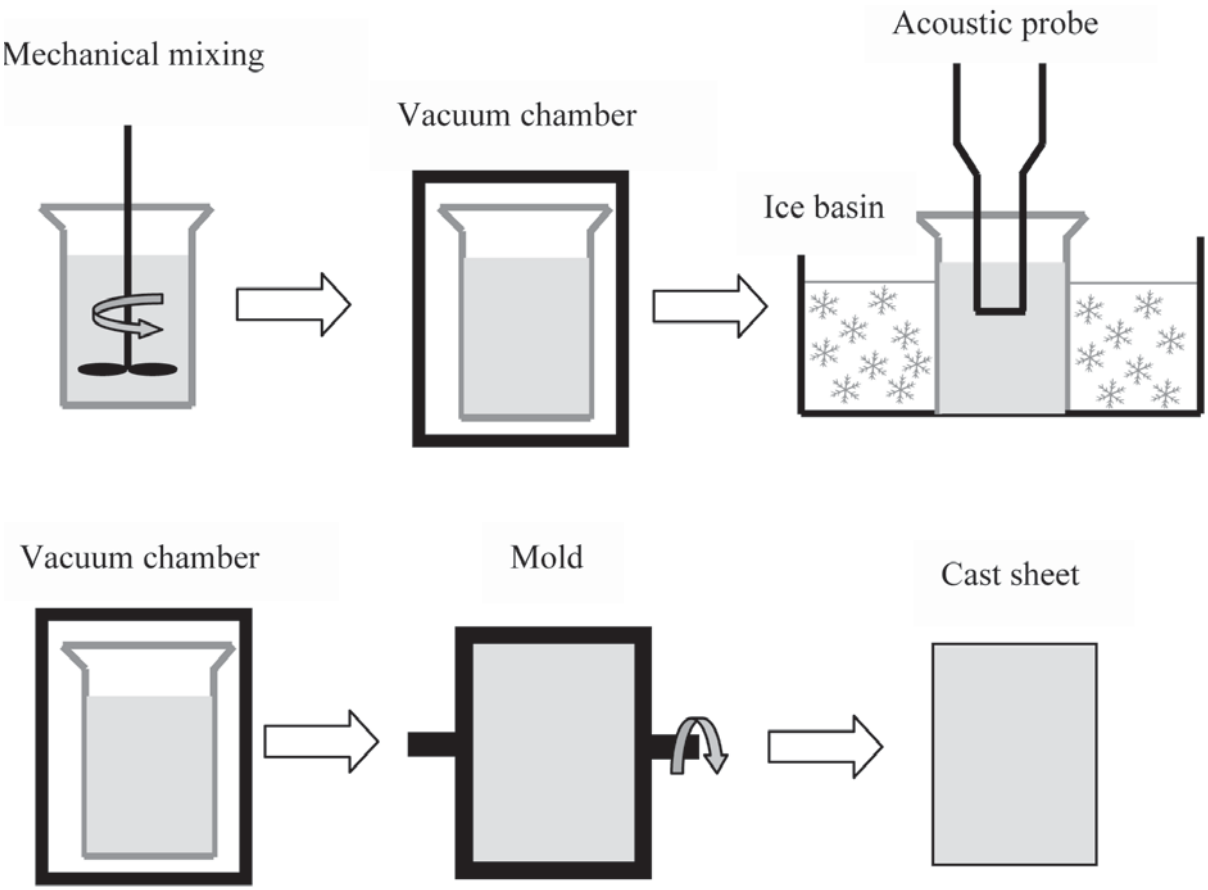

Fig. 1. Schematic of nanocomposite fabrication process.

quired volume percentage and mechanically mixed in a glass beaker for approximately 5 min. The mixture was then placed in a vacuum chamber at 28 Torr for 5 min to remove trapped air bubbles generated during the mechanical mixing process. After the deaeration process, the mixture was poured into a stainless steel beaker surrounded by an ice enclosure, and a 20 mm diameter acoustic probe from a Vibra-Cell ultrasonic processor resonant at 20 kHz was used to disperse the nanoparticles throughout the resin. Ultrasonic energy was employed for 70 min in the pulsing mode (10 sec on, 10 sec off) for an effective sonication time of 35 min. Although pulsing was primarily used to inhibit heat build-up in the specimen, it additionally enhanced material processing by allowing the material to settle back under the probe after each ultrasonic burst. The ice enclosure was simultaneously used to inhibit heat build up.

After the sonication process, the required amount of the hardner (0.85% w/w methyl ethyl ketone peroxide (MEKP) and 0.03% w/w cobalt octate for poly-

Table 2. Fracture properties of nanocomposites.

Material	K_{IC} (MPa-$\sqrt{m}$)	K_{ID} (MPa-$\sqrt{m}$)
Polyester (PO)	0.54	0.74
TiO_2+PO	0.85	0.95
Al_2O_3 +PO	0.86	0.91
Epoxy	0.67	0.84
Epoxy+platelet	1.03	-

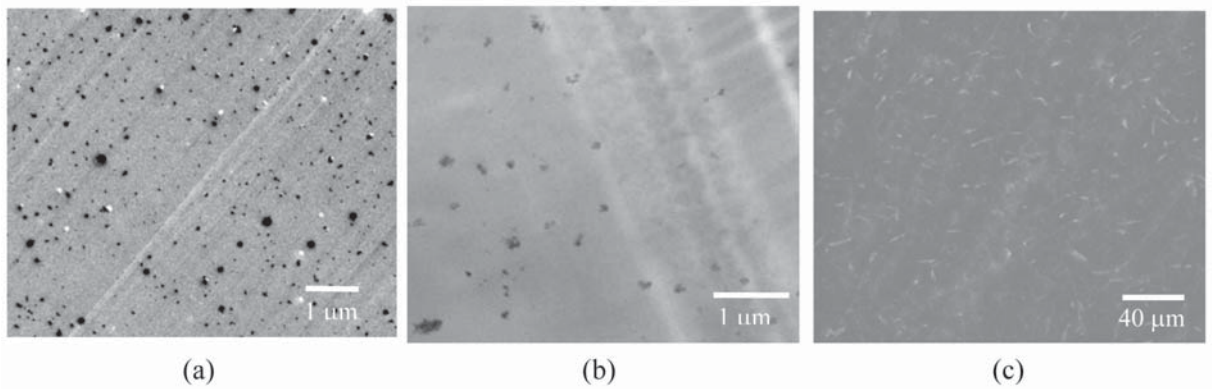

Fig. 2. TEM/SEM images showing dispersion of reinforcements (a) TiO_2 nanoparticles, (b) Al_2O_3 nanoparticles, (c) Al_2O_3 platelets.

ester and 10% w/w HY551 for epoxy) was added to the mixture and mixed thoroughly to initiate and accelerate the polymerization process. In the case of polyester resin the mixture was briefly deaerated at 28 Torr to remove trapped air bubbles generated during the sonication process. The brevity of the second deaeration process was necessary as polymerization commences almost immediately after the hardening agents are added. The second deareation was not done for epoxy as the gelation time for this resin was only 40 minutes. The final mixture was poured into a rectangular mold lined with thin (0.18 mm) mylar sheets to obtain smooth flat surfaces. In order to prevent particle settlement at the bottom, the mold was rotated at 2 rpm for at least 6 hours until the mixture was rigid enough so that particles could no longer migrate. The resin mixture was allowed to cure at room temperature for 72 hours. After this time, the specimen was taken out from the mold and post-cured in an air-circulating oven. For polyester samples the post curing was done for 4 hours at 52 °C followed by 5 hours at 63 °C. For the epoxy samples the post curing involved 2 hours at 100 °C. After allowing the oven to cool down to room temperature, the specimens were taken out and machined to desired shapes. The fabrication evolution is shown schematically in Fig. 1

From the results of previous investigations [8], the maximum improvement in fracture toughness was obtained for 1% volume fraction of the particle, and hence only this case is considered in this study. For nanoparticle samples, transmission electron microscopy (TEM) analysis was conducted to verify the level of nanoparticle dispersion in the matrix. For the platelet samples, scanning electron microscopy (SEM) was employed to inspect the dispersion, as the platelets are larger. The micrographs shown in Fig. 2 indicate that for 1% volume fraction, the fabrication procedure employed produced composites with excellent particle dispersion.

3. STATIC AND DYNAMIC INITIATION TOUGHNESS

The quasi-static plane strain fracture toughness of virgin polyester, epoxy and the respective composites were determined following ASTM D 5045-99. The dynamic fracture toughness of the composites

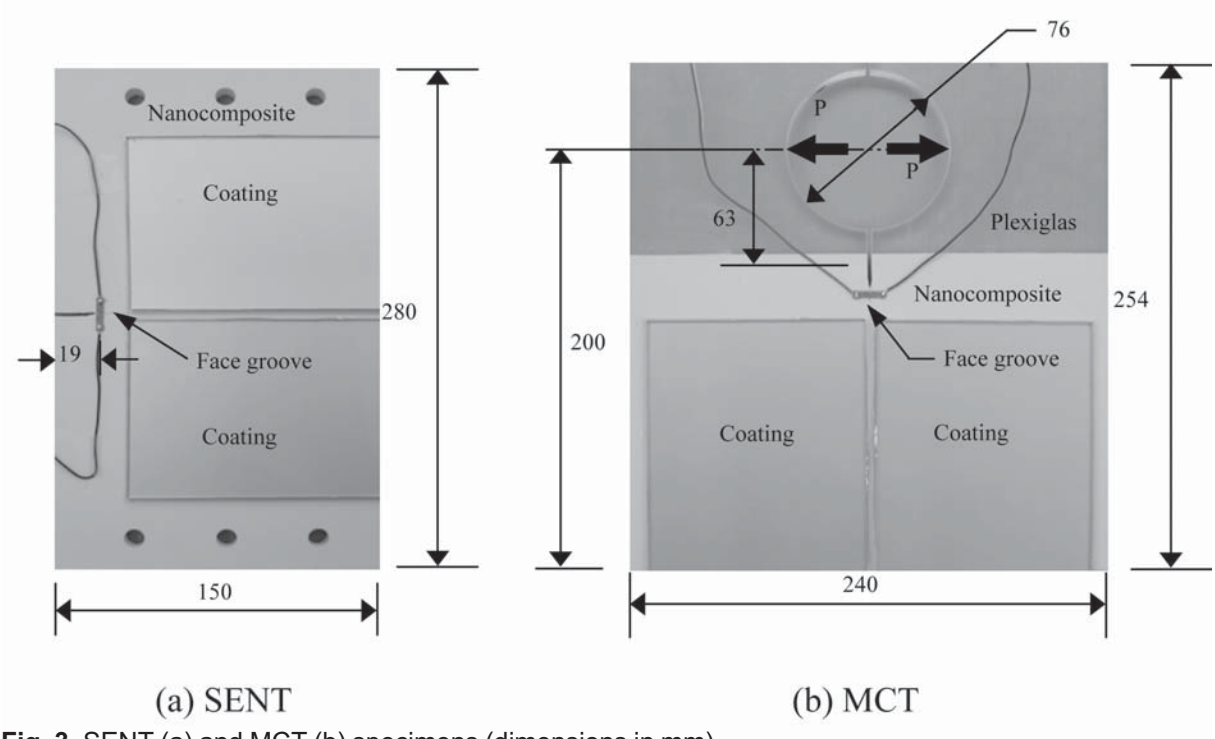

Fig. 3. SENT (a) and MCT (b) specimens (dimensions in mm).

was determined using the modified Hopkinson bar technique. The details of this method can be found elsewhere [8]. The quasi-static fracture toughness (K_{IC}) and the dynamic initiation toughness (K_{ID}) for the resins and the composites are listed in Table 2. The addition of nanoparticles improved the static fracture toughness of polyester by about 60%. In the case of the platelet, their addition also results in 60% improvement in static fracture toughness. The dynamic fracture toughness of the matrix material as well as the nanocomposites is found to be higher than their static counterpart by about 30% (the dynamic fracture toughness of the platelet composite has not been determined with confidence yet).

4. DYNAMIC CRACK PROPAGATION IN NANOCOMPOSITES

4.1. Specimen geometry and preparation

As mentioned earlier, once the crack becomes unstable and starts propagating, the fracture behavior is characterized in terms of the crack-speed versus dynamic stress intensity factor relationship ($\dot{a}$-K_D). After initiating, the crack may propagate at constant speed, accelerate and eventually branch or decelerate and arrest. For linear elastic fracture, the dynamic stress intensity factor K_D gives a direct measure of the energy expended in crack extension. So the parameters of interest are K_D and speed at which the crack will branch or the K_D at which the crack would arrest (arrest toughness K_A). A wide regime of crack speeds is to be covered to develop this relationship. Conventionally two different test specimen geometries are used; 1) the Single Edged Notch Tension (SENT) geometry and 2) the Modified Compact Tension (MCT) geometry. These two geometries are depicted in Fig. 3. The SENT is an increasing stress intensity factor (K) geometry for which K increases as the crack length increases, where as the MCT is a decreasing K geometry and will facilitate observation of crack arrest phenomena.

Nanocompostite sheets of the required size were prepared and the SENT and MCT specimens were machined out of these sheets to the final dimensions shown in Fig. 3. The MCT specimen was composed of sheets from two different materials, Plexiglas and nanocomposite. The two-part speci-

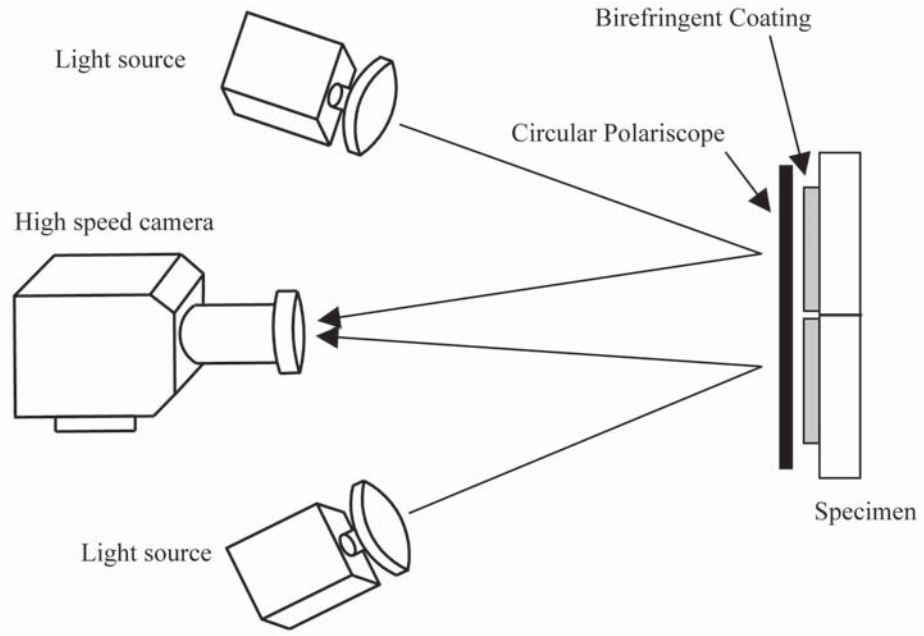

Fig. 4. Photoelastic setup for dynamic fracture study of nanocomposites.

men was used due to the limitation on the size of nanocomposite that could be made with good particle dispersion using the technique previously discussed. Plexiglas was chosen as a suitable mating part because of its compatibility with polyester/epoxy in terms of density and modulus. The circular hole was made on the separate sheet of Plexiglas, and the two pieces were bonded using fast curing epoxy adhesive. The crack was subsequently machined. Starter notches were made on all specimens with a band saw and were subsequently made blunt. The starter notch had a normalized length, a/W (W is the specimen width), of 0.125 for the SENT and 0.31 for the MCT specimen. In order to ensure that the crack propagated in a straight line, shallow face grooves were made on both sides of the specimens. Crack detection gages (CD-02-10A, Micro Measurements Inc., USA) were bonded near the starter notch to detect the initiation of fracture. Two identical photoelastic coatings of 3 mm thickness (Micro Measurements Inc., Raleigh, USA) were bonded on either side of the face groove using a fast curing epoxy adhesive. The coating made of polycarbonate had an elastic modulus of 2.48 GPa, a Poisson's ration of 0.36 and the optical fringe constant (f_σ) of 7000 N-/m-fringe.

4.2. Experimental details

The dynamic stress intensity factor (DSIF), K_D, for propagating cracks is usually measured from the crack tip mechanical fields. In the present study the technique of reflection photoelasticity combined with high-speed photography was employed to record the dynamic fracture. A schematic of the experimental setup is shown in Fig. 4. Xenon flash lamps were used as light sources to illuminate the specimen in the reflection mode. A circular polarizer sheet was placed in front of the specimen to create a dark field circular polariscope. Sixteen photographs of the dynamic event were recorded using an Imacon 200 high-speed digital camera at an exposure time of 200 nanoseconds. The photographs were taken at predefined time intervals of typically 15 μs for the SENT and 25 μs for the MCT. The SENT specimens were loaded to failure using an INSTRON machine whereas the MCT specimens were loaded using a special loading fixture as shown in Fig. 3. The camera was triggered using a crack detection gage mounted slightly down stream of the starter notch. As the crack propagated, the gage broke resulting in a potential drop and this potential drop was used to trigger the camera. The photographs were subsequently analyzed to determine

the crack speed and the dynamic stress intensity factor as explained in the next section.

4.3. Analysis of experimental data

The isochromatics obtained from the technique of photoelasticity are contours of constant maximum in plane shear stress, τ_{max}, which is related to the in plane principal stresses, σ_1 and σ_2 as follows [12].

$$\tau_{\max} = \frac{\sigma_1 - \sigma_2}{2} = \sqrt{\left(\frac{\sigma_{yy} - \sigma_{xx}}{2}\right)^2 + \sigma_{xy}^2} = \frac{Nf_\sigma}{2h}, \quad (1)$$

where, N is the fringe order and h is the specimen thickness and σ_{ij}, $i,j \in \{x,y\}$ are the inplane stress components. For a crack propagating at a constant velocity, c, the expansion of the stress field is given by Irwin [13]. The stress field has the general form given below

$$\begin{aligned}
\sigma_{xx} &= D\Big\{\left(1+2\lambda_1^2-\lambda_2^2\right)\mathrm{Re}\,\Gamma_1 - \frac{4\lambda_1\lambda_2}{\left(1+\lambda_2^2\right)}\mathrm{Re}\,\Gamma_2 + \\
&\left(1+2\lambda_1^2-\lambda_2^2\right)\mathrm{Re}\,\mathrm{Y}_1 - \left(1+\lambda_2^2\right)\mathrm{Re}\,\mathrm{Y}_2\Big\} \\
\sigma_{yy} &= D\Big\{-\left(1+\lambda_2^2\right)\mathrm{Re}\,\Gamma_1 + \frac{4\lambda_1\lambda_2}{\left(1+\lambda_2^2\right)}\mathrm{Re}\,\Gamma_2 + \\
&\left(1+\lambda_2^2\right)\left(\mathrm{Re}\,\mathrm{Y}_2 - \mathrm{Re}\,\mathrm{Y}_1\right)\Big\} \\
\sigma_{xy} &= D\Big\{2\lambda_1\left(\mathrm{Im}\,\Gamma_2 - \mathrm{Im}\,\Gamma_1\right) - \\
&2\alpha_l\,\mathrm{Im}\,\mathrm{Y}_1 + \frac{\left(1+\lambda_2^2\right)^2}{2\lambda_2}\mathrm{Im}\,\mathrm{Y}_2\Big\}, \qquad (2) \\
D &= \frac{1+\lambda_2^2}{4\lambda_1\lambda_2 - \left(1+\lambda_2^2\right)^2}; \\
\lambda_1 &= 1-\frac{\rho c^2}{c_l^2},\ \lambda_2 = 1-\frac{\rho c^2}{c_s^2},
\end{aligned}$$

where c_l and c_s are the dilatational and shear wave speeds in the material. The complex functions Γ_1, Γ_2, Y_1, and Y_2 in Eq. (2) are defined as a series as follows

$$\begin{aligned}
&\Gamma_1(z_1) = \sum_{n=0}^{N} C_n z_1^{n-1/2} \text{ and } \Gamma_2(z_2) = \sum_{n=0}^{N} C_2 z_1^{n-1/2} \\
&\mathrm{Y}_1(z_1) = \sum_{m=0}^{M} D_m z_1^m \text{ and } \mathrm{Y}_2(z_2) = \sum_{m=0}^{M} D_m z_2^m
\end{aligned} \qquad (3)$$

where $z_1=x+i\lambda_1 y$, $z_2=x+i\lambda_2 y$, $i=\sqrt{-1}$ and (x, y) are the coordinates with respect to the moving crack tip for a crack propagating in the x direction. In Eq. (3) the constant C_0 is related to the opening mode DSIF, K_D, as $K_D=C_0\sqrt{(2\pi)}$ and D_0 is related to the constant nonsingular stress acting parallel to the crack. Substituting Eqs. (2) and (3) in Eq. (1) gives a direct relationship between the DSIF and the fringe order. A set of data points around the crack tip are sampled from the isochromatics along with their corresponding fringe order and the DSIF is extracted from this data set using a non-linear over-deterministic least square scheme. For details of this method the reader is referred to Dally and Riley [12].

In the technique of reflection photoelasticity, the fringes are formed in the coating. The principle of coating technique premises that there is perfect strain transfer between the specimen and the coating. Thus, one has to transfer the results obtained from the coating back to the specimen, and also account for the additional reinforcement of the specimen by the coating. The reinforcement correction factor is defined as

$$F_{CR} = 1 + \frac{h^C E^C\left(1+\upsilon^S\right)}{h^S E^S\left(1+\upsilon^C\right)}, \qquad (4)$$

where E is the Young's modulus, ν is Poisson's ratio, h is the thickness, and the superscripts c and s refer to the coating and specimen, respectively. While using the coating, the light traverses through the coating twice and therefore the h in Eq. (1) is equal to $2h^c$. The stress intensity factor obtained by analyzing the fringes corresponds to the coating stresses and can be transferred to the specimen by the following equation [12].

$$K_D^S = F_{CR}\frac{E^S\left(1+\upsilon^C\right)}{E^C\left(1+\upsilon^S\right)}K_D^C. \qquad (5)$$

Typical isochromatics obtained from both SENT and MCT experiments are given in Figs. 5 and 6, respectively. The fringes converge at the crack tip. From the photographs, the crack tip location history is generated first, and using this information

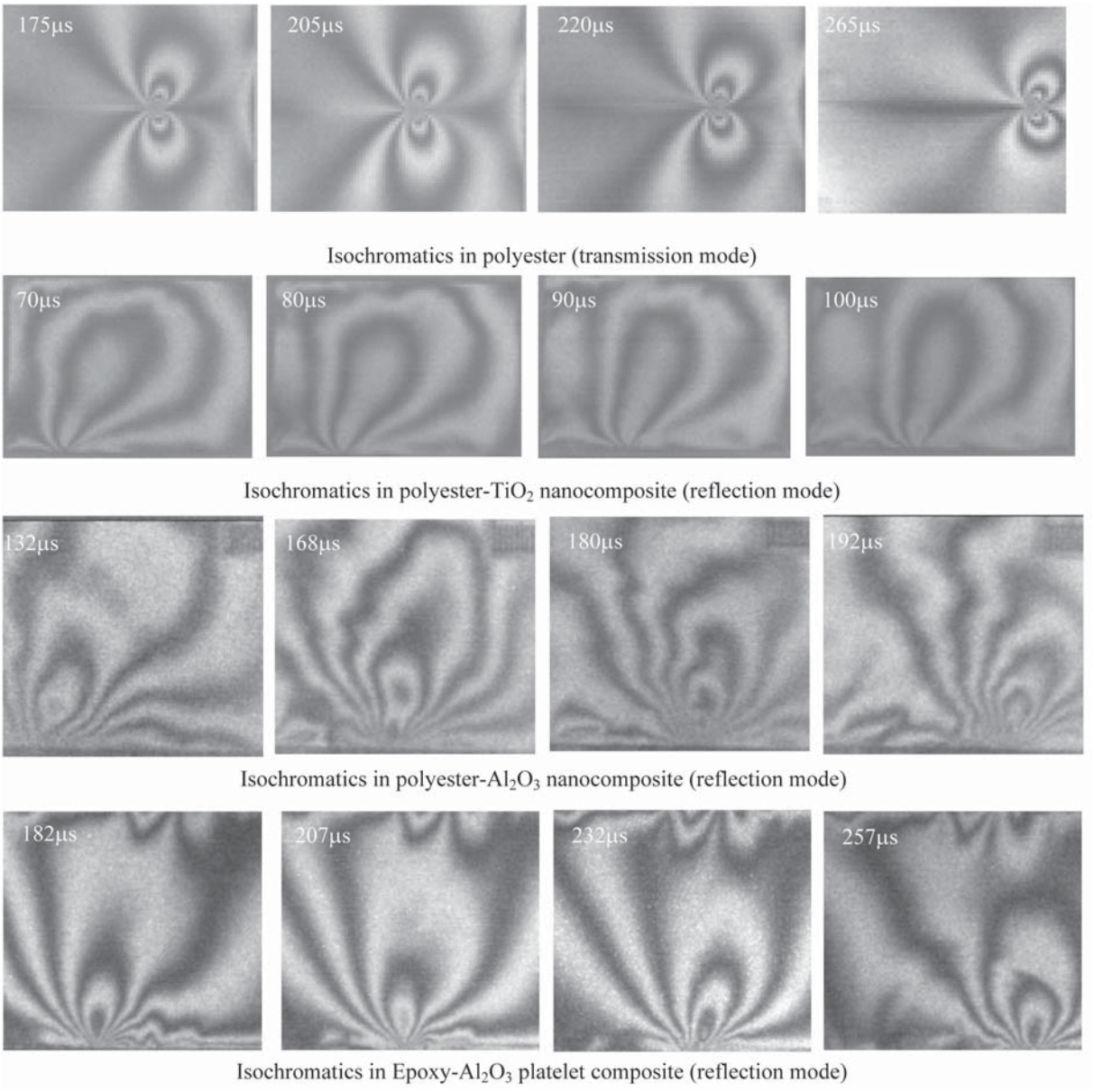

Fig. 5. Isochromatics obtained for SENT test (Only one half of the specimen is shown in the case of reflection mode).

and the time sequence of the photographs; the instantaneous crack speeds were obtained.

5. RESULTS AND DISCUSSION

5.1. Crack speeds

Typical crack tip location histories for the SENT and MCT experiments are shown in Fig. 7. The crack propagated at a constant velocity in the SENT experiments where as in the MCT tests, the crack initially propagated with constant speed and then decelerated and arrested. The maximum crack speed for polyester was 435 m/sec, which is about 38% of the shear wave speed in the material. For the polyester nanocomposites with TiO_2 nanoparticles the highest crack speed attained was 695 m/sec; 63% of the shear wave speed. In the case of Al_2O_3-polyester composites the maximum crack speed was 640 m/sec. For the epoxy- Al_2O_3 plate-

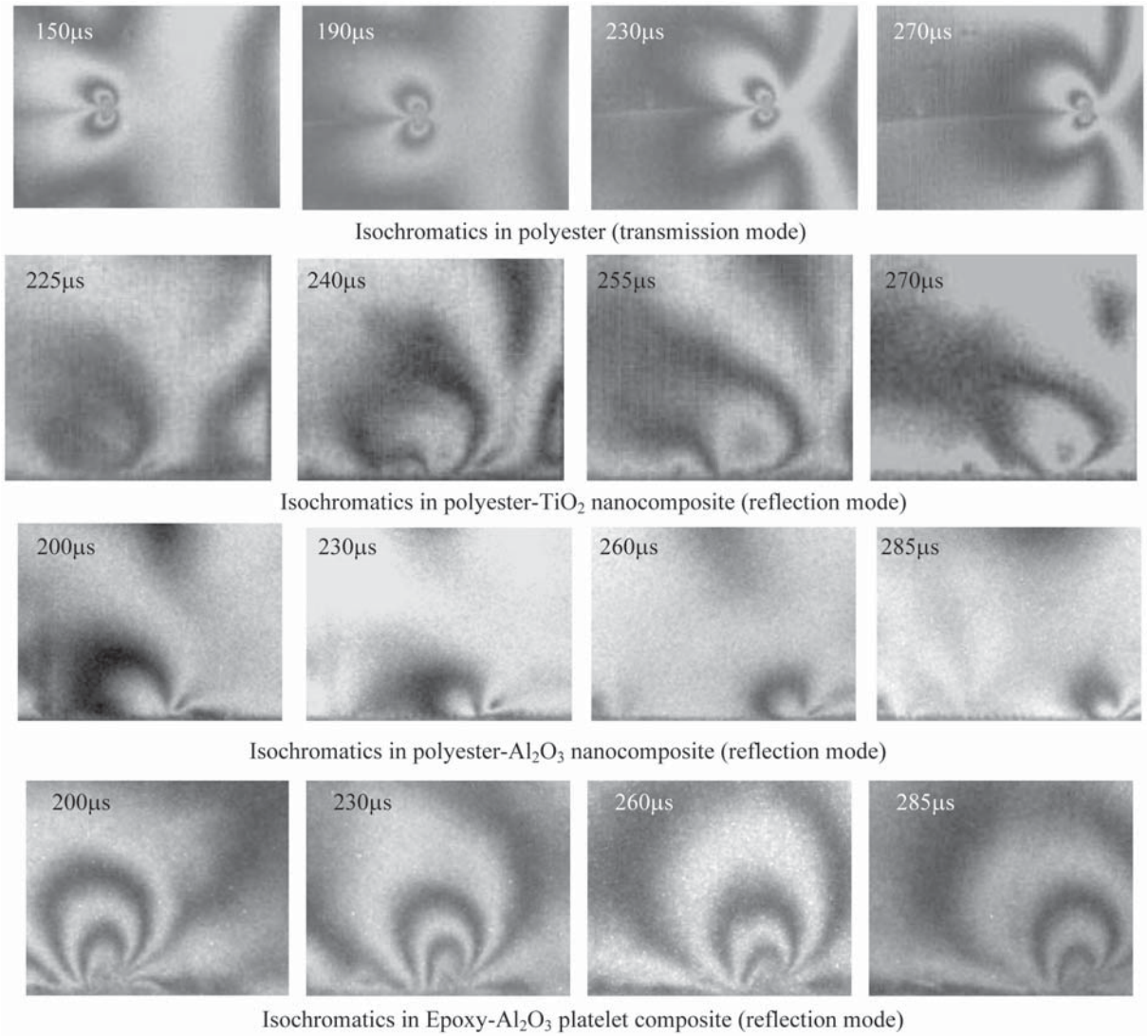

Fig. 6. Isochromatics obtained for MCT test (Only one half of the specimen is shown in the case of reflection mode).

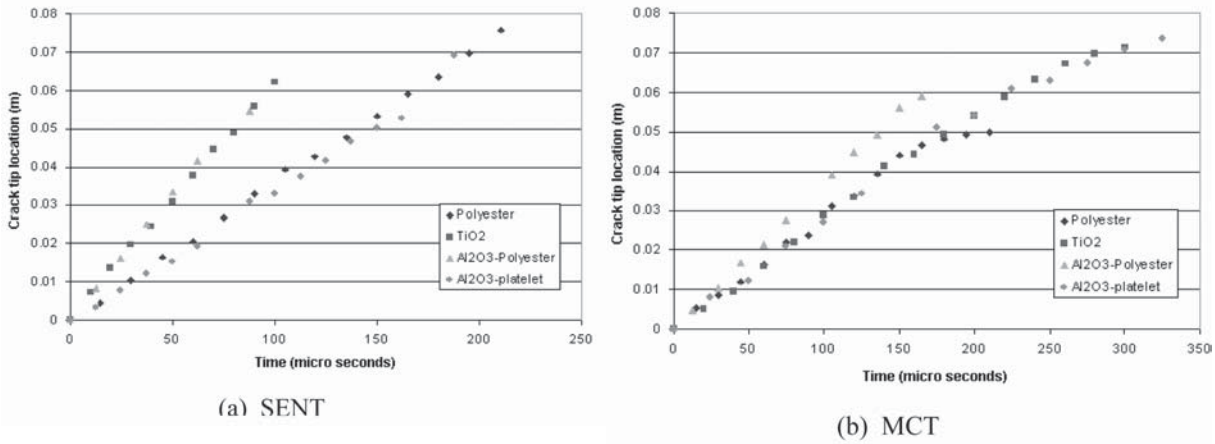

Fig. 7. Typical crack-tip location history for SENT and MCT experiments for polyester and composites (the time is shifted such that the first photograph corresponds to *t*=0 seconds for which a=0).

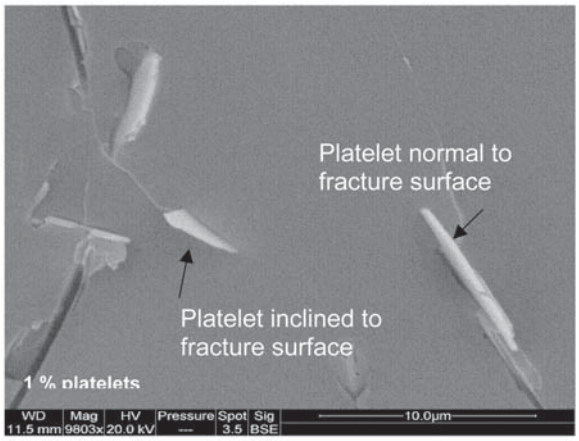

Fig. 8. SEM images of the fracture surface showing normal and inclined platelet pull out.

let composites, the highest crack speed attained was only 30% of the shear wave speed in the epoxy, i.e. 355 m/sec. Among the four different materials considered, the platelet composite has the highest fracture toughness, followed by the two nanocomposites.

Brittle polymers like polyester and epoxy when subjected to far field loading, the terminal crack speeds attained before crack branching are about 35% of the shear wave speed for polyester and about 30% of the shear wave speed for epoxy [11]. For the TiO_2 and Al_2O_3 nanocomposites, the observed crack speeds are higher in the rage of 60% of the shear wave speed. The crack speed history depends primarily on the stress intensity factor (K_Q) to which the initially blunt crack is loaded, the specimen geometry (SENT or MCT) and the propagation toughness and arrest toughness of the material. It is believed that the presence of nanoparticles which are considerably smaller in size (14 and 35 nm) inhibit crack branching and facilitates higher crack propagation velocities even though the shear wave speed in polyester and the nanocomposites are very close. Also there are additional mechanisms of energy dissipation in nanocomposites by way of interfacial debonding which will not allow the local energy density at the propagating crack tip to reach the level required for branching even at speeds exceeding 40% of the shear wave speed.

The case of platelet composites is quite the opposite. In the platelet composites, the highest crack speed observed is about 30% of the shear wave speed, which is the same as that for pure epoxy. Contrary to the nanopartilces, the platelets having size in the 5-10 μm range and thickness of 200 nm can provide considerable crack closure forces. In particular, platelets that are inclined to the fracture surface will not pull out cleanly even after they debond, hence can provide crack bridging until there is matrix spallation or platelet fracture. Fig. 8 is an SEM image of the fracture surface showing normal and inclined platelet pull out. Additionally platelets are more effective in crack deflection than spherical particles. All these can reduce the rate of crack front extension and therefore the observed maximum crack speed is also low.

5.2. $\dot{a}$-K_D relationship

In the SENT experiments, the crack propagation is at more or less constant speed whereas the DSIF shows a steady increase with the crack extension. In the MCT experiments, the crack eventually slows down and arrests and the DSIF decreases with crack extension. Combining these two data, one can construct a constitutive curve indicating the dependence of the crack speed on the DSIF. A plot of the crack speed as a function of the DSIF is shown in Figs. 9 to 11 for all the nanocomposites considered in this study.

All the materials considered in this study exhibit a universal trend in the $\dot{a}$-K_D variation. The relationship shows two distinct regions, namely, a vertical stem region where the crack speeds up rapidly for small changes in DSIF and a horizontal region where the DSIF changes rapidly for small changes in crack velocity. The continuous curve corresponding to each set of data points shown in the figure is a mean trend curve drawn for clarity of explanation. The intersection of this curve with the *x* axis provides the value of the arrest toughness. The arrest toughness values inferred accordingly are 90%, 95%, 65%, and 85% of the respective quasi-static fracture toughness for polyester, TiO_2 nanocomposite, Al_2O_3 nanocomposite, and the epoxyplatelet composites, respectively. In the case of the platelet composites, the dependence of the DSIF on crack speed is stronger and becomes weak only at the maximum speed of 0.3 c_s.

6. CONCLUSIONS

Polymer nanocomposites were prepared using two different thermosetting resins, polyester and epoxy,

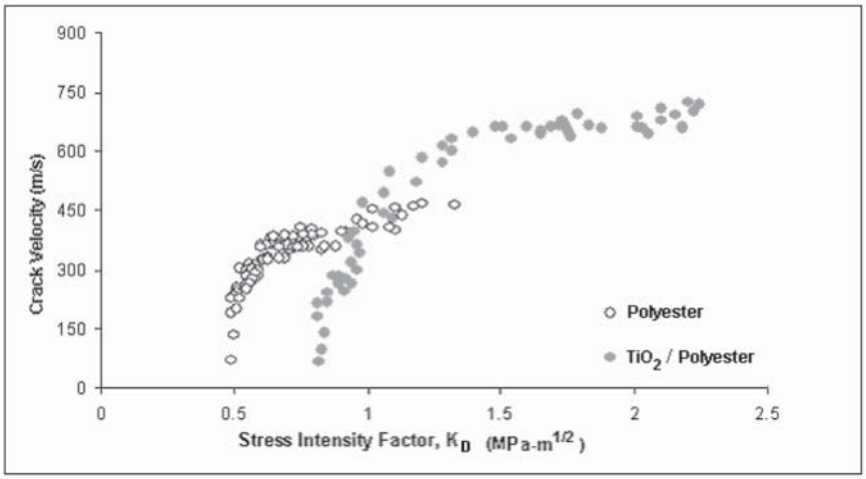

Fig. 9. Crack-speed *c* versus dynamic stress intensity factor K_D relationship for polyester and TiO_2/ Polyester nanocomposites.

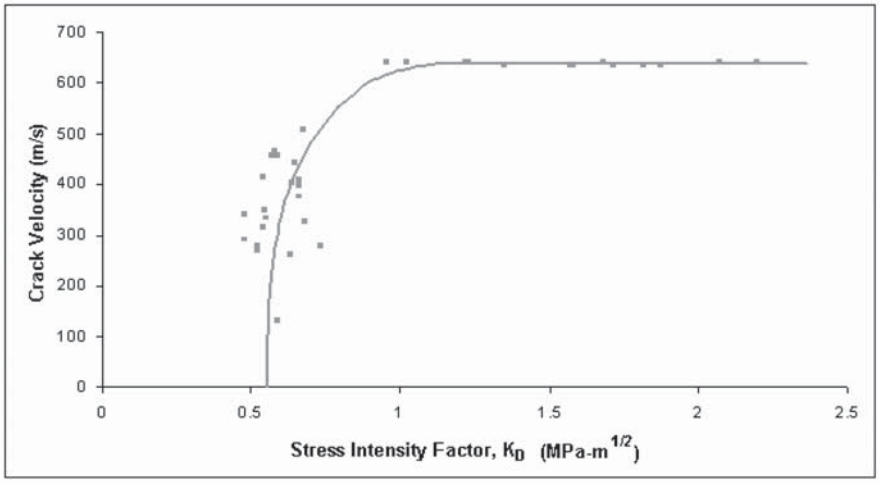

Fig. 10. Crack-speed c versus dynamic stress intensity factor K_D relationship for Al_2O_3/Polyester nanocomposites.

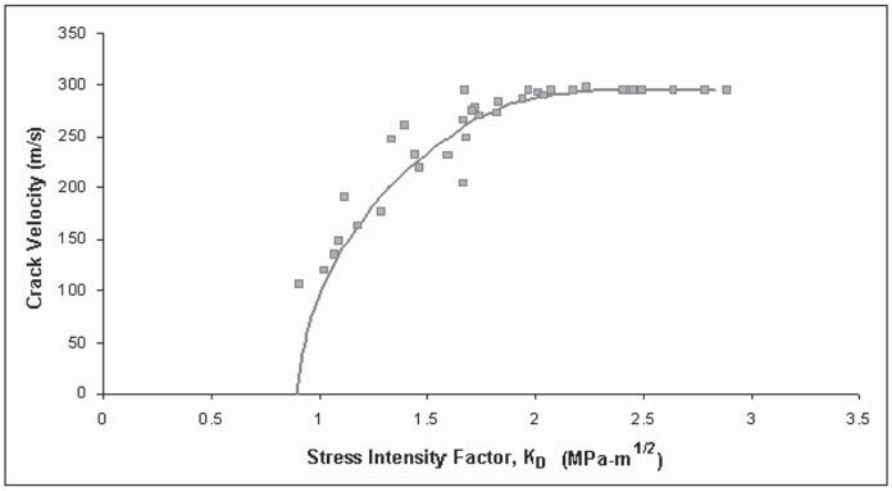

Fig. 11. Crack-speed c versus dynamic stress intensity factor K_D relationship for Polyester/Al_2O_3 platelet nanocomposites.

with three different particles of varying sizes and shape as reinforcements. The composites were characterized for their quasi-static and dynamic fracture initiation toughness. The addition of the particles was shown to improve the fracture resistance of the material. Furthermore, a comprehensive set of experiments was conducted to investigate the behavior of propagating cracks in these materials using two different crack geometries. The results indicated that the crack speeds in the nanocomposites containing the particles were 50% higher than that observed in the virgin resin. The platelet composite on the other hand did not exhibit this behavior.

ACKNOWLEDGEMENTS

The authors would like to acknowledge the support of NSF under grant no. CMS 0244330, INT 0422767 and DST under grant number DST/INT/US-NSF/RPO-159/04.

REFERENCES

[1] A. J. Kinloch, S. J. Shaw, D. A. Tod and D. L Hunston // *Polymer* **24** (1983) 1341.
[2] A. G. Evans, S. Williams and P. W. R. Beaumont // *Journal of Materials* Science. **20** (1985) 3668.
[3] B. Geisler and F. N. Kelley // *Journal of Applied Polymer Science* **54** (1994) 177.
[4] A. J. Kinloch, M. L. Yuen and S. D. Jenkins // *Journal of Materials Science* **29** (1994) 3781.
[5] M. Hussain, A. Nakahira, S. Nishijima and K. Niihara // *Materials Letters* **27** (1996) 21.
[6] R.P. Singh, M. Zhang and D. Chan // *Journal of Materials Science* **37** (2002) 781.
[7] M Zhang and R. P. Singh // *Materials Letter* **58** (2002) 408.
[8] V.M.F. Évora and A. Shukla // *Mater. Sci. and Eng*. **A361** (2003) 358.
[9] S. C. Zunjarrao, R Sriraman and R. P. Singh // *Journal of Material Science* **41** (2006) 2219.
[10] T. Kobayashi and J. W. Dally // *ASTM STP 711* (1980) 189.
[11] J. T. Metcalf and T. Kobayashi // *ASTM STP 711* (1980) 129.
[12] J. W. Dally and W. F. Riley, *Experimental Stress Analysis*, 4th Edition (College HomeEnterprises, 2005).
[13] G. R. Irwin, Series representation of the stress field around constant speed cracks (University of Maryland Lecture Notes, 1980).